Structure and Dynamics of the β-Barrel of the Membrane Transporter BtuB by Site-Directed Spin Labeling†

Gail E. Fanucci,‡ Nathalie Cadieux,§ Christie A. Piedmont,‡ Robert J. Kadner,*,§ and David S. Cafiso*,‡

Department of Chemistry and Biophysics Program and Department of Microbiology, University of Virginia, Charlottesville, Virginia 22901

Received April 9, 2002; Revised Manuscript Received July 19, 2002

ABSTRACT: Site-directed spin labeling and EPR spectroscopy were used to map two consecutive β-strands of the putative transmembrane β-barrel of BtuB. For these studies, a series of 29 consecutive single cysteine mutants of BtuB were produced covering residues 148−176. The proteins were then expressed, reacted with a sulfhydryl-specific spin label, purified in octyl glucoside (OG), and reconstituted into palmitoyloleoylphosphatidylcholine (POPC) bilayers. The labeled residues spanned from the extracellular region (position 148) to the small periplasmic loop (positions 160−163) and back up to the extracellular side (position 176) of BtuB. Continuous wave power saturation in the presence of oxygen or NiAA yielded an $i, i + 2$ periodicity for the collision frequencies at these sites and demonstrated the presence of a β-strand structural motif. For both strands studied, the even-numbered residues were found to be exposed to the hydrophobic phase of the bilayer, whereas the odd-numbered residues pointed toward the interior of the barrel and the core of the protein. In addition, the collision parameters yielded the position of the protein within the bilayer. The phase relationship between the oxygen and metal collision frequencies along with the corresponding membrane depth parameters, Φ, indicates that segments 151−159 and 164−172 are within the bilayer. In POPC bilayers, there is a mobility gradient for spin labels along the barrel indicating enhanced backbone flexibility toward the periplasmic surface of the barrel. In POPC/OG mixed micelles, the even-numbered residues facing the hydrocarbon show an increased mobility compared with the bilayer environment whereas the inward-facing side chains show little change in motion. The data indicate that the protein core remains folded in POPC/OG mixed micelles but that this environment increases the backbone fluctuations of the strands. A model for the β-barrel of BtuB is presented in part on the basis of these EPR data.

The outer membrane (OM)[1] of Gram-negative bacteria contains a family of membrane proteins that function to transport nutrients from the extracelluar medium into the periplasmic space. BtuB is a 66 kDa protein (594 amino acids) found in the outer membrane that functions in the active transport of vitamin B_{12}, and it belongs to a family of OM active transport proteins, such as FepA, FhuA, and FecC, that are dependent upon the transperiplasmic protein, TonB (*1*−*4*). In these TonB-dependent transporters, transport of the substrate into the periplasmic space is achieved by coupling the substrate-loaded OM transporter to the TonB complex, which consists of the inner membrane proteins TonB, ExbB, and ExbD. This protein−protein interaction drives putative conformational changes in the OM transporter by extracting energy from the protonmotive force of the inner membrane. This active transport machinery can be contrasted to the passive diffusion of small molecules that takes place through the porins of the outer membrane (*2*, *5*).

The overall mechanism of TonB-dependent transport is not well understood, but several features of the transport process have been characterized. A better understanding of the transport phenomenon has been dramatically advanced by the X-ray crystallographic structure determination of three iron transport proteins, FepA, FhuA, and FecA (*6*−*9*). The structures of these proteins each consist of an outer β-barrel formed from 22 antiparallel β-strands that surround the N-terminal globular domain that forms a core or hatch region (see Figure 1). Additionally, TonB-dependent transporters contain a highly conserved region (6 residues) close to the N-terminus called the Ton box (*10*). The transport process begins when substrate binds near the rather large extracellular loops of the outer membrane receptor. The addition of substrate results in a dramatic conformational change of the Ton box segment, causing its extension into the periplasm where it is then available to interact with TonB (*11*, *12*).

† This work was supported by NIH Grants GM35215 to D.S.C. and GM19078 to R.J.K. and NIH NRSA Postdoctoral Fellowship GM20298 to G.E.F.

* Correspondence should be addressed to D.S.C. at the Department of Chemistry, University of Virginia, P.O. Box 400319, Charlottesville, VA 22904-4319, or R.J.K. at the Department of Microbiology, University of Virginia School of Medicine, Charlottesville, VA 22908-0734.

‡ Department of Chemistry and Biophysics Program.

§ Department of Microbiology.

[1] Abbreviations: CNCbl, cyanocobalamin; DPPH, α,α′-diphenyl-β-picrylhydrazyl; DTT, DL-dithiothreitol; EPR, electron paramagnetic resonance; GUVs, giant unilamellar vesicles; HEPES, *N*-(2-hydroxyethyl)piperazine-*N*′-2-ethanesulfonic acid; MTSL, *S*-(1-oxy-2,2,5,6-tetramethylpyrroline-3-methyl)methanethiosulfonate; NiAA, nickel(II) acetylacetonate; PCR, polymerase chain reaction; OM, outer membrane; PMSF, phenylmethanesulfonyl fluoride; SDSL, site-directed spin labeling; POPC, 1-palmitoyl-2-oleoyl-*sn*-glycero-3-phosphocholine; OG, *n*-octyl pyranoglucoside.

10.1021/bi0259397 CCC: $22.00
Published on Web 09/04/2002

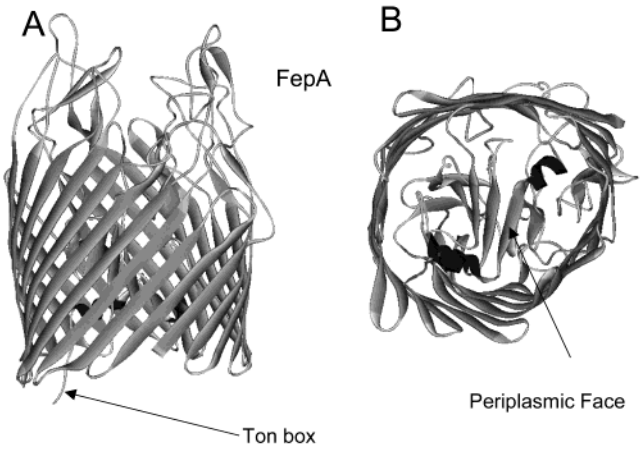

FIGURE 1: Crystal structure of FepA (PDB id: 1FEPA) as viewed (A) from the side of the barrel and (B) toward the periplasmic surface of the transporter (*6*). The Ton box is shown in an extended conformation, and substrate binds in the loop regions on the extracellular surface.

The Ton box is not resolved in the FhuA crystal structure, but the first helix, H1, unfolds in the presence of substrate (*7*). This event is believed to provide a signal to TonB that the outer membrane protein is loaded with substrate, resulting in the binding of TonB to the transporter (*11*, *13*). Although the Ton box is shown in the FepA crystal structure as an extended strand, previous site-directed spin-labeling (SDSL) experiments on BtuB (residues 6−12) indicate that the Ton box segment is restrained within the barrel of the transporter in the absence of substrate and that its conformation becomes extended only after substrate addition (*12*). It is likely that the unfolding of the Ton box when substrate is bound can be generalized to the iron transport proteins. The subsequent events in the transport process, including how TonB interacts with the transporter along with passage of the substrate through the protein, remain unclear; however, these events may involve a rearrangement or unfolding of the core of the transporter to produce a channel through which substrate may pass (*13*−*15*).

Although a high-resolution crystal structure for BtuB has not been described, its overall structure is expected to be similar to the OM iron transporters. Additional structural information comparing these proteins is clearly desirable because BtuB has a significantly shorter sequence. Site-directed spin labeling (SDSL) has the potential to provide information on the secondary structure of BtuB, specifically elucidating or confirming the transmembrane arrangement of the β-strands and β-barrel configuration. In general, SDSL has proven to be an extremely powerful spectroscopic approach to examine protein structure, protein dynamics, and protein conformational changes (*16*, *17*). This method is of particular value for larger membrane proteins, such as BtuB, which may not be amenable to NMR techniques. Although SDSL has been used quite frequently to study helical structures (*18*−*21*), fewer studies have been performed on β-sheets (*16*, *22*), and only one study on the spectroscopy of spin labels placed along a membrane β-barrel structure has been reported (*23*). In this case a putative transmembrane β-strand was scanned in FepA with spin labels, and power saturation was used to correctly identify β-strand 5 in the barrel prior to elucidation of the crystal structure.

In the present work, two putative strands in the β-barrel of BtuB are investigated by SDSL. The strands were chosen on the basis of sequence homology with FepA and FhuA and the known structures of these two transporters. This work was carried out with several objectives in mind. The first was to identify and confirm that the structure of BtuB consists of transmembrane β-strands consistent with a β-barrel configuration and to position the barrel strands within the lipid bilayer. A second goal was to identify residues that face the interior of the barrel and those that face the membrane hydrocarbon. A third goal was to investigate the dynamics of residues that span the interior and exterior of the β-barrel region and, finally, to expand the data set for EPR spectra of spin labels placed on β-barrel sites. The work presented here confirms that the labeled sites form transmembrane β-strands consistent with a barrel structure for BtuB and provides information about the organization of the barrel strands within the bilayer. Furthermore, a model for the BtuB barrel was generated from a combination of the EPR data, the crystal structures for FepA and FhuA, and the results from a predictive algorithm for barrel propensities (*24*). In addition, inspection of the EPR data from exposed spin labels on the BtuB strands indicates that the dynamics of the spin-label side chain varies along the length of the strands and that the periplasmic end of the barrel is more dynamic than the extracelluar end. Finally, the data demonstrate that protein dynamics are altered in a selective manner when the protein is removed from lipid and placed into a mixed detergent/lipid micelle environment.

EXPERIMENTAL PROCEDURES

Materials

The sulfhydryl-reactive spin-labeled methanethiosulfonate, *S*-(1-oxy-2,2,5,6-tetramethylpyrroline-3-methyl)methanethiosulfonate (MTSL), was purchased from Toronto Research Chemicals (Ontario, Canada). Nickel(II) acetylacetonate hydrate (NiAA) was obtained from Aldrich Chemical Co. (Milwaukee, WI), DL-dithiothreitol (DTT) was from Sigma (St. Louis, MO), sarkosyl was from Fisher Chemical Co. (Pittsburgh, PA), and phenylmethanesulfonyl fluoride (PMSF) was purchased from Boehringer Mannheim Corp. (Indianapolis, IN). Octyl glucoside (Anagrade) was purchased from Anatrace (Maumee, OH). 1-Palmitoyl-2-oleoyl-*sn*-glycero-3-phosphocholine was purchased from Avanti Polar Lipids (Alabaster, AL).

Methods

Mutagenesis and Isolation of Intact Outer Membranes. A two-step PCR-based site-directed mutagenesis technique that has been described previously was used to produce cysteine mutants in BtuB (*11*). The mutants were expressed in *Escherichia coli* in strain RK5016 (*metE*), which is a derivative of strain MC4100 [Δ(*argF*-*lac*)*U*169 *araD*139 *rpsL*150 *relA*1 *flbB*5301 *deoC*1 *ptsF*25 *rbsR*22 *non*-9 *gyrA*219] having the additional mutations *metE*70 *argH btuB recA* and which requires vitamin B_{12} in order to synthesize methionine. To test for functionality, the different mutants were grown on minimal A salt agar supplemented with 0.02% glucose, 0.01% Arg, and various concentrations of

vitamin B_{12} (0.1−5000 nM) in place of methionine. The comparison was made with growth on similar plates containing 0.01% Met, as previously described (*25*). All the BtuB Cys mutants were therefore tested for their ability to use vitamin B_{12} in place of methionine for growth. They were all found to function as well as the wild-type protein in this growth assay. Outer membranes were isolated as described previously (*14*). Briefly, following centrifugation at 4000*g* for 10 min, the cells were resuspended in HEPES, pH 6.5, and lysed using a French press running at a pressure of 18000 psi. The suspension contained PMSF at a final concentration of 20 μg/mL to prevent degradation of BtuB. After lysis, the solution was centrifuged for 10 min at 14500*g* to remove cellular debris, and the inner membranes in the supernatant were solubilized by addition of 0.5% sarkosyl. The outer membranes containing BtuB were then pelleted by ultracentrifugation for 1 h at 100000*g*, resuspended in 4 mL of HEPES buffer at pH 6.5, and washed by one additional centrifugation.

Protein Purification and Spin Labeling. For spin labeling and purification the OM were solubilized by OG with the following procedure. Typically, 4 mL of the OM fragments containing BtuB was added to12 mL of buffer (25 mM Tris, 5 mM DTT, 0.05 mM EDTA, pH 8.0) containing 0.7 g of OG. The final volume of buffer was adjusted to 50 mL. The sample was incubated at 37 °C for 10 min, then allowed to sit at room temperature for 1 h, and then pelleted by ultracentrifugation for 1 h at 100000*g*. The supernatant was retained and used for spin labeling and purification. A significant amount of the BtuB protein was found in the pellet, but no attempt was made to isolate or characterize that fraction of the protein.

All BtuB mutants were spin labeled before purification by ion-exchange chromatography. Typically, half of the supernatant was labeled and purified at a time; hence, to 30 mL of supernatant was added 100 μL of 22 mM MTSL solution. The spin-labeling reaction proceeded for 2−17 h before purification by FPLC.

Protein samples were purified in a single chromatographic step. FPLC was performed using an AKTA purifier system (Amersham Biosciences) with a 5 mL HP Seph Q prepacked column. In a typical elution profile the column was equilibrated with 30% B (buffer A, 25 mM BisTris and 16 mM OG, pH 7.0; buffer B, 25 mM BisTris, 16 mM OG, and 1 M LiCl, pH 7.0), loading sample, washing with 5 column volumes of 30% B, and eluting with two different gradients, first from 30% to 80% B in 7 column volumes and then 80−100% B in 1 column volume. The minor contaminants were collected in the sample flow-through, and the major contaminant, most likely OmpA, eluted around 35−40% B, whereas BtuB eluted at 75−85% B. The purity of samples was determined by SDS−PAGE. Silver staining revealed that lipopolysaccharides were present in the purified BtuB fractions, but the levels of LPS relative to BtuB were not quantitated.

Liposome Reconstitution and Sample Preparation. Purified protein samples were reconstituted by the dialysis of OG from mixed POPC/OG micelles (*26*). Typically, 20 mg of POPC was mixed with 80 mg of OG in 2 mL of buffer (10 mM HEPES, 130 mM NaCl, pH 6.5) and sonicated until clear. FPLC fractions (2−14 mL) containing 0.5−2 mg of BtuB were added to the mixed micelle solution, allowed to sit at room temperature for 1 h, and then dialyzed against six 4 L buffer changes (10 mM HEPES, 130 mM NaCl, pH 6.5, 1 μM EDTA, 0.25 mM NaN_3). Following dialysis, the samples were pelleted by centrifugation at 34000*g* at 4 °C for 30 min. No protein could be detected in the supernatant either by SDS−PAGE or by EPR spectroscopy. Previous work indicates that dialysis from OG produces primarily large unilamellar vesicles (*27*−*29*), and we believe this to be the case here. Because the lipid-to-protein ratios are in excess of 500:1, BtuB is unlikely to affect the vesicle morphology.

The pellet of reconstituted BtuB was resuspended in 100 μL of the supernatant and then further concentrated to 50 μL using a Beckman Airfuge. The typical sample size for EPR measurements is 5−8 μL so each preparation provided enough material for four to five different measurements. For the power saturation experiments, 4.7 μL of sample and 1.3 μL (100 mM) of NiAA were mixed to approximate a 20 mM NiAA solution. For measurements with B_{12}, 5 μL of sample was mixed with 1 μL of a B12 stock solution to give a final B_{12} concentration of 450 μM. In both cases, multiple freeze−thaw cycles were performed to ensure that the added reagents had an equal distribution on the inside and outside of the vesicles. For measurements in mixed micelles, typically 2 μL of reconstituted BtuB in POPC was mixed with 2 μL of an OG stock to give a final molar ratio of 17:1 OG:POPC.

Electron Paramagnetic Resonance. EPR spectroscopy was performed on a Varian E-line 102 series X-band spectrometer equipped with a loop-gap resonator (Medical Advances, Milwaukee, WI). Labview software was used for data collection and analysis and was generously provided by Drs. Christian Altenbach and Wayne Hubbell (UCLA). For lineshape analyses, all spectra were recorded at 2.0 mW incident power from samples prepared in glass capillary tubes with a 0.8 mm i.d. (VitroCom, Mountain Lakes, NJ). For power saturation measurements, the samples were placed in gas-permeable TPX tubes (Medical Advances, Milwaukee WI), and saturation of the resonance was carried out with a microwave power that varied from 0.25 to 100 mW. During these experiments, either a stream of air (oxygen accessibility) or nitrogen (baseline measurement and metal relaxing agent) was used to purge the samples. The $P_{1/2}$ values, which are related to the product $(T_{1e}T_{2e})^{-1}$, were then determined from the power saturation curves as described elsewhere (*30*). The $P_{1/2}$ values were used in turn to determine the collision parameter Π for each reagent. The parameter Π is related to the change in T_{1e} of the nitroxide and the frequency of collision of either NiAA or O_2 with the R1 side chain (*31*). Finally, the membrane depth parameter, Φ, was determined from the ratios of the $\Delta P_{1/2}$ for each reagent as described previously (*32*).

RESULTS

EPR Line Shapes Reveal the BtuB β-Barrel Structure and Its Two Surfaces. BtuB lacks native cysteine residues, and incorporation of a single cysteine residue by site-directed mutagenesis produces a reactive site to attach the spin-label side chain R1 (Scheme 1). Shown in Figure 2 are a series of EPR spectra corresponding to the R1-labeled single cysteine substitutions scanned throughout two putative β-strands. Efficient labeling of cysteines with the MTSL probe was

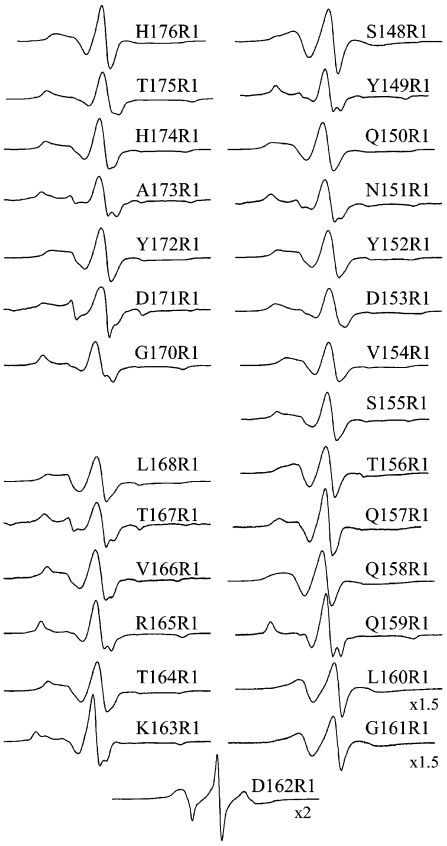

FIGURE 2: EPR spectra of the spin-labeled R1 side chain scanned along two sequential putative β-strands within the β-barrel of BtuB. The stack plots are arranged according to strand with the top of the figure representing the extracellular side of the protein and the bottom representing the periplasmic side. All spectra were acquired with a 100 G sweep width at 2 mW incident microwave power with a modulation amplitude of 1.0 G (peak to peak). The *y*-axes for mutants D162R1, G161R1, and L160R1 were divided by factors of 2, 1.5, and 1.5, respectively, to fit these spectra uniformly in the figure.

Scheme 1

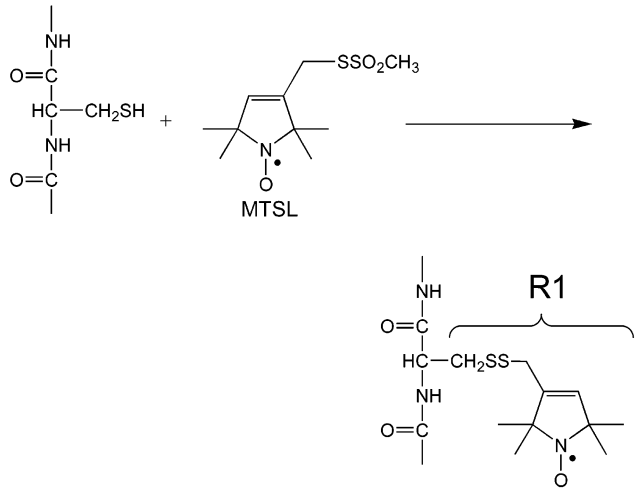

achieved for each site in detergent-solubilized BtuB, except at position 169, which appears to be buried facing the core of the protein near the bilayer center (see below). The spectra in Figure 2 are grouped according to strand with the top of the figure indicating those residues positioned near the extracellular side of the protein. Inspection of the EPR line shapes indicates that a wide range of nitroxide mobility is

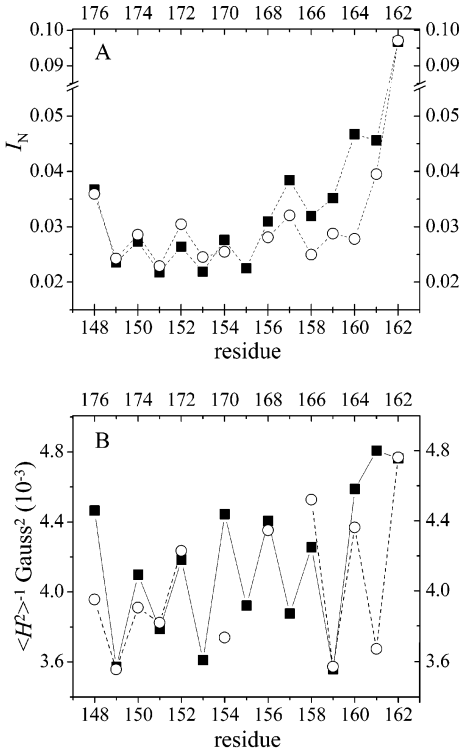

FIGURE 3: (A) Plot of the normalized amplitude, I_N, of the central first-derivative resonance of the EPR spectra. (B) Plot of the inverse second moment of each of the EPR spectra shown in Figure 2. In both (A) and (B), residues 176−162 (○) and residues 148−162 (■) are plotted (left to right) from the extracellular to periplasmic side of the protein.

reflected in these spectra. In the present case, our use of the term "mobility" includes both the effects of local order and rate of motion of the nitroxide side chain. In general, the contributions of rate versus order are hard to separate (see Discussion), but several qualitative conclusions can be made for the spectra in Figure 2. For example, relatively narrow line shapes are observed for R1 at positions 160−162 that arise from large amplitude motions that occur on the nanosecond time scale. These line shapes are similar to those found for the R1 side chain when placed into flexible loops (*19*). In contrast, the EPR spectra for several positions, for example, 159, 165, and 173, are very broad and indicate that the R1 side chain is undergoing motions that are restricted in space, resulting in spectral line shapes that approach the theoretical rigid limit. These rigid limit spectra are expected for labeled sites buried within hydrophobic regions of proteins. It is apparent in Figure 2 that the EPR spectra for R1 are broadest and less mobile for the odd-numbered residues in both strands. This effect is most clearly observed for residues 148 through 160 but not as apparent for the second strand.

In general, the mobility of the nitroxide side chain is reflected in the relative breadth of the EPR spectrum (*19*), and two ways to measure the breath of the spectra are plotted in Figure 3. Figure 3A shows plots of the normalized amplitude of the central transition line of each EPR spectrum, and Figure 3B shows the calculated reciprocal second moments of each of the line shapes in Figure 2. Both plots clearly show an i, $i + 2$ periodicity in these parameters. It is also apparent from Figure 3 that the mobility of the R1 label is greatest for those residues on the C-terminal end of the

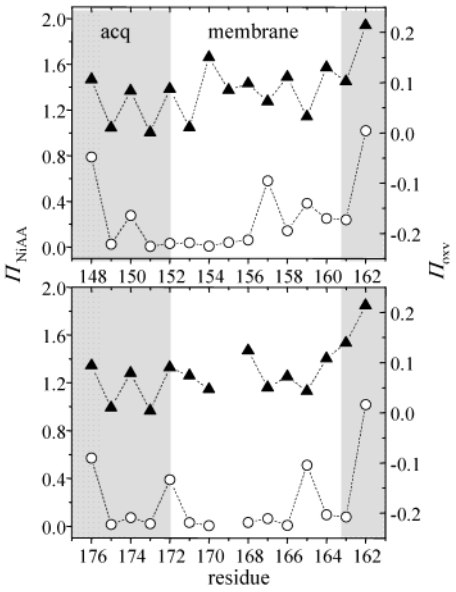

FIGURE 4: Collision accessibilities (Π) for oxygen (▲) and NiAA (○) for two putative β-strands in BtuB determined using air (20% oxygen) and 20 mM NiAA, respectively, with a nitrogen gas purge as background. The shaded regions correspond to those residues that are in the aqueous phase. A β-strand (i, $i + 2$) periodicity is clearly revealed in these data. The values of Π_{NiAA} and Π_{oxy} are in phase for portions of the protein exposed to the aqueous phase but are out of phase for protein within the membrane domain (see text for discussion).

first strand scanned and the N-terminal end of the second, which both lie near the periplasmic side of the protein. The i, $i + 2$ periodicity is maintained for those residues that are expected to extend into the extracellular loops (see below), and this periodicity pattern indicates that these segments maintain a β-strand structure beyond the bilayer. The increase in side-chain mobility toward the periplasmic side of the strands most likely results from an increase in backbone fluctuations near the periplasmic surface (see Discussion). From the normalized intensity pattern shown in Figure 3, the even-numbered residues, which have a higher degree of side-chain mobility, are assigned to the exterior barrel surface. On the other hand, the odd-numbered residues, which have generally broader EPR spectra, are assigned to the interior surface facing the core or hatch region of the barrel. These assignments are further supported by the results of power saturation measurements shown below.

Paramagnetic Collision Parameters Position the Two β-Strands across the Bilayer. Shown in Figure 4 are the collision parameters, Π, for each residue in the presence of air (20% O_2) or 20 mM NiAA. The Π values are directly related to the frequency of collisions between paramagnetic O_2 or NiAA and the nitroxide (*31*) and can be related to the relative location of the spin label. For each putative strand region scanned, there is a strong i, $i + 2$ correlation for the Π values, again indicating a β-strand structure. At the ends of these segments, the Π values for O_2 and NiAA are in phase (for example, positions 148−151 and positions 176−173). This in-phase behavior is consistent with a β-strand structure that extends into the aqueous phase, and the corresponding regions are shaded in Figure 4. An extension of the β-strand structure past the extracellular side of the membrane has been observed in many other β-barrel OM proteins of Gram-negative bacteria (*5*), and it can be seen

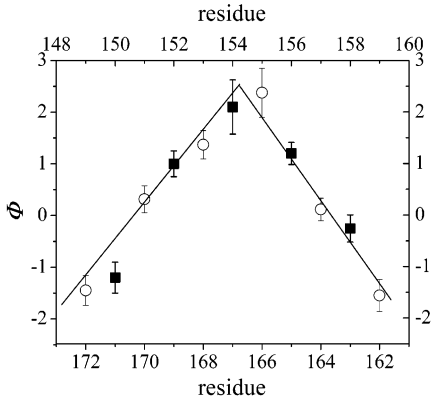

FIGURE 5: The bilayer depth parameter, Φ, plotted as a function of residue number for each strand. Data are shown only for the hydrocarbon facing (even-numbered) residues that span the bilayer. Residues 148−162 (■) and 176−162 (○) are plotted (left to right) from the extracellular to the periplasmic surface of the protein.

in Figure 4 that both of the strands in BtuB retain their secondary structure significantly past the membrane environment. Residues that lie within the membrane domain should have Π values for O_2 and NiAA that are out of phase. For a transmembrane β-strand in a β-barrel, an out-of-phase relationship between the Π values for O_2 and NiAA is predicted because of the differences in O_2 and NiAA concentrations in the hydrocarbon compared to the aqueous phase (*16*). The O_2 levels are highest in the center of the bilayer whereas the NiAA concentration approaches a minimum in the bilayer and is highest in the aqueous phases. Additionally, the core of the barrel more closely resembles an aqueous environment with a high NiAA concentration and with O_2 levels approaching a minimum value. The contrasting environments on the opposite sides of a strand lead to an i, $i + 2$ pattern for Π values that are out of phase and identify the orientation of the strand in the barrel. This pattern is expected to be a signature of a β-strand of a β-barrel that spans a membrane. For those residues in the central region of the strands (for example, positions 156−160), an out-of-phase behavior for the values of Π for O_2 and NiAA is indeed observed. For the even-numbered residues, the values of Π for O_2 increase while the values of Π for NiAA decrease, indicating that the even-numbered residues point toward the hydrocarbon environment. For the odd-numbered residues that point toward the core of the protein, the values of Π for NiAA are expected to be high; however, many low NiAA Π values are obtained and indicate that side chains that face the protein core are buried and hence inaccessible to the metal complex.[2]

Figure 5 shows the depth parameters, Φ, for each of the labeled positions that face the exterior of the BtuB barrel. The values of Φ for the residues at the end of the strands approach values expected for a spin label located in the bulk aqueous phase (≈ −2) (*33*). On the other hand, maximum values of Φ are measured for residues 154, 156 and residues 166, 168, indicating that these residues are located in the

[2] It should be noted that although both of these strands have odd-numbered residues pointing inward with even-numbered residues pointing toward the bilayer phase, there is no requirement that all of the strands in the barrel follow this pattern. The large extracellular loops are variable in length, and clearly the numbering in this case is a coincidence.

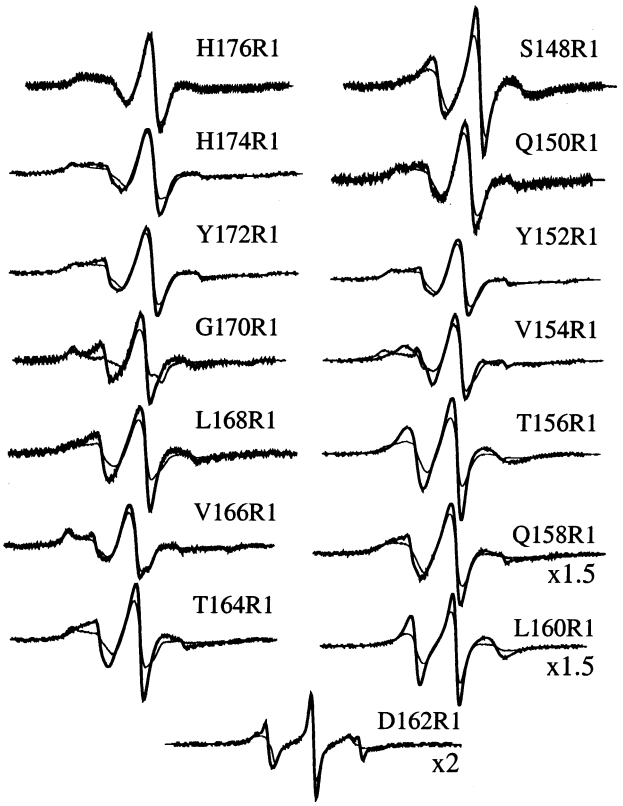

FIGURE 6: Stack plots of the EPR spectra for even-numbered mutants reconstituted into POPC bilayers (thin lines) and in mixed POPC/OG micelles (thick lines). The two columns separate the spectra according to β-strand and are arranged (top to bottom) from the extracellular to the periplasmic protein surface. The *y*-axes for mutants D162R1 and L160R1 were divided by factors of 2 and 1.5, respectively, to scale these spectra into the figure.

center of the bilayer. These findings demonstrate that the strands are transmembrane and that the shaded regions in Figure 4 are aqueous. Further, these results also support the idea that the in-phase and out-of-phase behaviors of the *i*, *i* + 2 collision probabilities shown in Figure 4 delineate segments that are within the bilayer region from those lying outside the membrane. The data in Figure 5 demonstrate that approximately 10 residues are required for these strands to transit the bilayer. This result is expected on the basis of the tilt of the β-strands in FepA and FhuA (*23*).

The Dynamics of the β-Barrel Are Altered in Mixed Micelles. In the present EPR study, the BtuB mutants were isolated, labeled in OG, purified, and then reconstituted into POPC from OG/lipid mixed micelles. The integrity and function of these reconstituted BtuB samples were confirmed by our ability to reproduce the conformational changes observed previously in the Ton box from samples prepared in intact outer membrane fragments (*12*) (data not shown). In the mixed micelle environment, we are able to effectively label sites that are not readily labeled in the OM sample (data not shown). To determine whether detergent enhances the labeling efficiency by altering either the structure or dynamics of BtuB, the effect of the detergent was investigated by resolubilizing the labeled reconstituted BtuB−POPC membrane with OG (see Methods). In this case, BtuB was placed in a mixed micelle environment having a POPC:OG molar ratio of 1:17. Figure 6 compares spectra for the even-numbered (hydrocarbon facing) residues in the mixed micelle

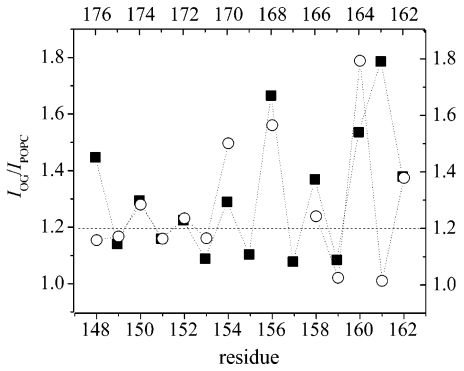

FIGURE 7: Plot of the ratios of the normalized central resonance intensities in mixed micelles to the intensities in POPC bilayers, I_{OG}/I_{POPC}. The data for residues 148−162 (■) and 176−162 (○) are plotted (left to right) from the extracellular to the periplasmic side of the protein.

with those in the POPC (reconstituted) environment. In the mixed micelle environment, the EPR line shapes were narrower and larger in amplitude in almost every case, indicating that the motion of the spin label has been enhanced. Relatively little or no change in the EPR line shape was detected for the odd-numbered residues. Figure 7 shows the ratio of the normalized EPR intensities in the presence and absence of OG (I_{OG}/I_{POPC}) for each residue along the two strands. Several features are immediately apparent from this plot. There are only minor changes in the normalized intensities of the EPR spectra for spin labels at the odd-numbered positions, with the exception of position 161, which is located in a small periplasmic loop of the BtuB barrel. For the even-numbered residues, the largest changes in the EPR line shapes for samples in the mixed micelles are observed near the periplasmic loop of the two β-barrel strands. Because the spectra for the inward-facing residues (odd-numbered sites) remain similar in line shape, the data in Figures 6 and 7 indicate that the protein remains folded in the presence of mixed POPC−OG micelles but that OG solubilization alters the dynamics of the BtuB barrel (see Discussion).

DISCUSSION

The SDSL data presented here clearly delineate two consecutive β-strands consistent with a β-barrel configuration for BtuB. The EPR results also position the segments of this outer membrane transporter within the membrane. Furthermore, the exterior and interior topology of the amino acid side chains is clearly revealed in these studies.

EPR spectra were previously obtained for a transmembrane β-strand in a related TonB-dependent iron transport protein, FepA (*23*). In that study, SDSL confirmed a β-strand secondary structure for a 9-residue segment and positioned the strand across the lipid bilayer. The data obtained here for BtuB, when compared to the data for FepA, show a much more dramatic variation in R1 dynamics as one scans though the β-strands. Although the line shapes for those residues facing the external side of the barrel (pointing into the lipid matrix) are similar to those of FepA, the internal EPR line shapes in BtuB show a much higher degree of immobilization. It should be noted that the sample preparation conditions for FepA and BtuB are not the same, but we do not believe that these differences account for the variability in line shape

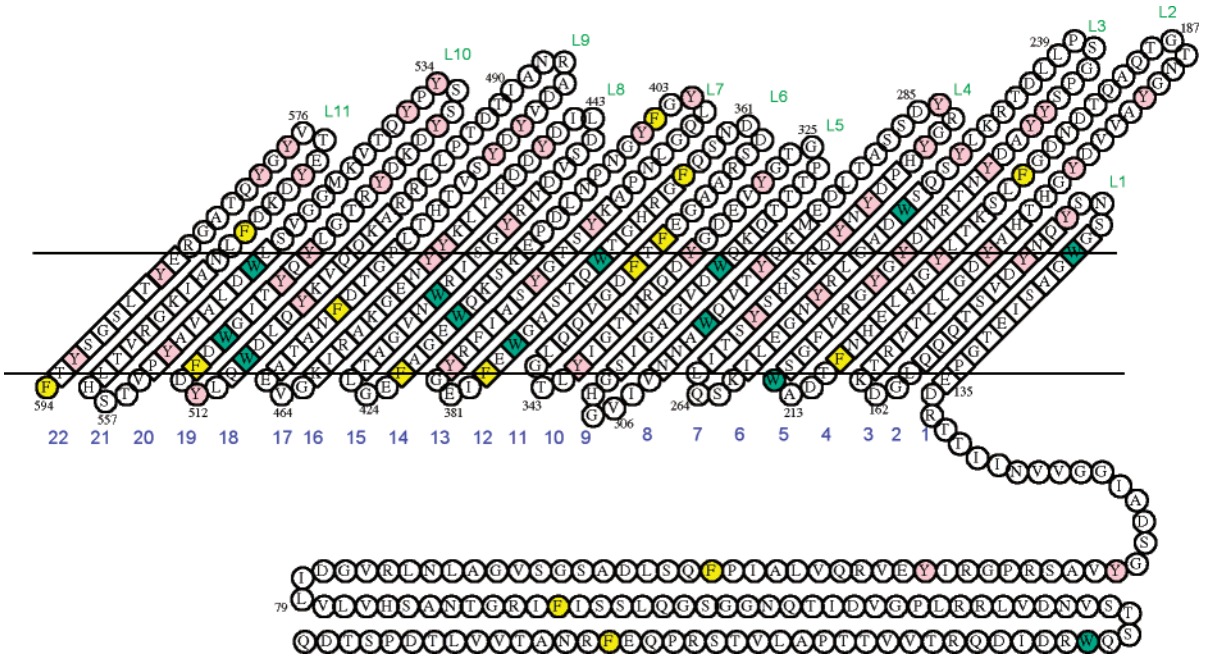

FIGURE 8: Putative model for the folding of the β-barrel of BtuB. The aromatic residues are shown colored, diamond-shaped residues refer to β-strand secondary structure, whereas the circular residues represent nondesignated secondary structure. The solid line defines the position of the phosphates at the bilayer interface as determined from the EPR power saturation measurements (see Results).

seen between the previous FepA study and those obtained here on BtuB. Both of these sample preparation procedures appear to result in proteins that are properly folded into the membrane. The difference in mobility for the internal-facing residues in BtuB and FepA is more likely to result from their strand number in the barrel. The residues in the FepA study, 245−253, are located in the fifth β-strand from the periplasmic side. In BtuB, we believe that residues 148−176 comprise the second and third strands in the barrel. Upon inspection of the crystal structure of FepA, the residues previously investigated by SDSL lie near the periplasmic side of strand 5 and make relatively few contacts with the core domain of the protein. In the FepA structure, strands 2 and 3 make more contacts with the internal domain. If strands 2 and 3 in BtuB have a homologous conformation to those in FepA, this additional steric crowding for the inward-facing side chain on strands 2 and 3 could be responsible for the more restricted label motion obtained here.

Determination of the structure of BtuB is clearly of interest in order to delineate the mechanisms leading to transport by this outer membrane protein. It will be of interest to know whether the structure of BtuB is analogous to that of other TonB-dependent transporters, and knowledge of the structure will facilitate further studies using SDSL to explore conformational changes and to elucidate the transport mechanism. A high-resolution structure for BtuB is not yet available, but we have combined the EPR results presented here along with the sequence homologies to FepA and FhuA and the results from a predictive algorithm for barrel-forming propensities of amino acid sequences to generate a model for the BtuB barrel structure.

An algorithm was recently reported that predicts the probability that a given 10 amino acid sequence forms a membrane-spanning β-strand (*24*). This algorithm provides a β-strand score for a sequence of 10 amino acids, examining their relative hydrophobicity, positioning of aromatic sites, and relative occurrence in known membrane-spanning β-strands of β-barrels. A score greater than 2 is judged to be a transmembrane β-strand. When the amino acid sequences of the barrel strands in FepA and FhuA are compared to those predicted by the algorithm for BtuB, there is a striking sequence conservation for some of the strands and an even stronger sequence conservation for the periplasmic loops. These similarities in sequence and the predicted β-strand scores make the model in Figure 8 reasonably convincing. This model represents our best guess at the barrel structure of BtuB with the diamond-shaped residues indicating the β-strand secondary structure and circles representing loops or hairpin turns. The solid lines represent the probable membrane bilayer interface. Placement of the line is determined from the EPR power saturation measurements of residues 148−176. Some error may be present in the exact positioning of the strands within the bilayer, as well as the exact identity of the residues in the start and end of the strands. However, as expected, most of the aromatic residues fall within the bilayer near the membrane interface. Compared to FepA (71.9 kDa) and FhuA (82 kDa), BtuB (66 kDa) has the least mass, and this pictorial view of the barrel and loops shows where the mass differences in BtuB compared to FepA and FhuA occur. In this model, BtuB, like FepA and FhuA, is formed from 22 antiparallel β-stands. The extracellular binding loops, particularly loops 5, 7, and 11 from FepA and loops 3, 4, and 5 from FhuA, are significantly shorter in the BtuB model. Interestingly, loop 2 in the BtuB model is similar in length to that found in FepA whereas loop 2 in FhuA is significantly shorter. Additionally, the exceptionally long β-strand segments of strands 7−12 in FhuA appear to be shortened in the structure of BtuB. In general, the largest differences in sequence homology and the greatest differences between the FepA and FhuA structures occur within the extracellular binding loops that interact with substrate. This is consistent with the idea that these proteins are adapted to different substrates but function by a common mechanism.

As indicated above, the mobility of the nitroxide label may describe both its rate of motion and its amplitude of motion or molecular order. Both rate and order affect EPR line shapes by altering the spacial averaging of the anisotropic magnetic interactions of the nitroxide. In general, it is difficult to separate these two contributions to the mobility, but recent reports describe the use of spectral simulations and motional models for the R1 side chain to obtain rates and order parameters from the spectra of certain labeled sites (*20*, *21*, *34*). Of importance in these studies was the finding that differences in label mobility for the exposed residues on helices were the result of differences in local backbone fluctuations (*20*). Differences in local backbone motion are important for helical sites because the motion of the nitroxide is not strongly influenced by interactions with nearby side chains. The results presented here for BtuB provide an interesting observation regarding the mobility of spin-labeled side chains along the length of the barrel. As shown in Figure 3, there is a trend toward increased label mobility from the extracellular to the periplasmic side of the membrane. Such a gradient would not be expected if these effects originated primarily from interactions with other side chains on the surface of the barrel. As a result, it is likely that the gradient of spin-label mobility observed for the even-numbered residues in the β-barrel of BtuB arises from a gradient in local backbone fluctuations. A definitive conclusion regarding this intriguing possibility will require further work to determine the exact origins of this trend and to determine if it is present in other strands in BtuB.

The observed gradient in label mobility is dramatically enhanced when the protein is placed into a mixed micelle environment, as shown in Figure 7. Because the size of the BtuB-mixed micelle complex is quite large, it is unlikely that an increased tumbling rate can account for the enhanced mobility of the R1 side chain. Furthermore, the effects of line narrowing from an increased correlation time should not have a large asymmetric effect upon the labeled sites in the protein. The change in label mobility is unlikely to result from a change in hydrocarbon chain order in the mixed micelle, because previous work on bacteriorhodopsin demonstrates that the R1 side chain on a protein surface is not sensitive to the gradient in molecular ordering that exists across the lipid bilayer (*30*). Increased mobility cannot be the result of protein unfolding because this protein remains folded in mixed micelles. Although the EPR line shapes of the outward-facing residues change significantly, those side chains that point toward the core exhibit only small changes in their mobilities. In general, those residues facing the core are more restricted in their motion as they are in strong tertiary contact. These broader line shapes are not expected to be strongly affected by backbone dynamics and therefore serve as monitors of protein unfolding. The simplest explanation for the selectively increased side-chain motion is that the backbone fluctuations at the periplasmic side of the strands are further enhanced in the mixed micelle. In the FhuA structure, approximately 9 salt bridges and 60 hydrogen bond contacts are made between the core and the barrel (*7*), whereas in FepA, there are 46 hydrogen bond interactions between the core and the barrel with another 17 interactions between the core and the binding loops (*6*). An increased aqueous accessibility to the protein interior and barrel in the presence of a mixed micelle may lead to the exchange of protein hydrogen bonds with water, which could account for the observed increased backbone fluctuations. These results demonstrate clear differences between a membrane protein in a mixed micelle versus membrane environment, and they suggest ways in which membrane proteins might be altered by these membrane mimetic systems.

Why should the periplasmic ends of β-strands in BtuB exhibit greater motion than the extracellular ends? The periplasmic end of the β-barrel of the TonB-dependent transporters FhuA and FepA does not make as many contacts with the protein core as does the extracelluar end, a structural feature that could account for the gradient in label mobility we detect in BtuB. The exterior loop regions may also play a role in stabilizing that end of the barrel. Is there any role for the enhanced motion seen toward the periplasmic end of BtuB? We speculate that the periplasmic side of the transporter, in particular, the periplasmic loops, may be designed to interact with the inner membrane protein TonB. Indeed, previous work on protein dynamics indicates that surfaces designed for protein−protein contact may be more dynamic than other regions of the protein (*35*−*37*). This enhanced dynamics may lead to an adaptive structure that is better suited to facilitate a protein−protein interaction.

It should be noted that, for the labeled sites investigated here, no differences in the EPR line shapes were observed in the presence of substrate (CNCbl) (data not shown). However, more definitive work investigating distances between labeled side chains across strands is currently in progress to look for structural changes that may take place in the barrel of the transporter upon the binding of substrate.

In summary, the data obtained here provide information on the structure and transmembrane arrangement of two putative β-strands within the barrel of BtuB. The data indicate that EPR spectra of R1 labels along β-barrel structures can be quite varied as a result of both tertiary contact within the barrel and backbone dynamics of the strands. From the EPR spectra, it is apparent that even-numbered residues face the exterior of the barrel, while odd-numbered residues point inward toward the protein core. Furthermore, the EPR spectra suggest that there is a gradient in backbone fluctuations across these β-strands and that the protein is more dynamic at its periplasmic face. Using these EPR data along with sequence homology with other TonB-dependent transporters and an algorithm to identify transmembrane β-sheets, a model for the barrel of BtuB has been generated.

ACKNOWLEDGMENT

We thank Prof. Bill Wimley for generously providing the results of his algorithm for the transmembrane β-strands of FepA, FhuA, and BtuB and Prof. Michael Wiener and his laboratory for providing assistance with the purification of BtuB.

REFERENCES

1. Moeck, G. S., and Coulton, J. W. (1998) *Mol. Microbiol. 28*, 675−681.
2. Klebba, P. E., and Newton, S. M. C. (1998) *Curr. Opin. Microbiol. 1*, 238−248.
3. Postle, K. (1999) *Nat. Stuct. Biol. 6*, 3−6.
4. Sansom, M. S. P. (1999) *Curr. Biol. 9*, R254−R257.
5. Ralf, K., Locher, K. P., and Van Gelder, P. (2000) *Mol. Microbiol. 37*, 239−253.

6. Buchanan, S. K., Smith, B. S., Venkatramanil, L., Xia, D., Esser, L., Palnitkar, M., Chakraborty, R., van der Helm, D., and Deisenhofer, J. (1999) *Nat. Struct. Biol. 6*, 56−63.
7. Locher, K. P., Rees, B., Koebnik, R., Mitschler, A., Moulinier, L., Rosenbusch, J. P., and Moras, D. (1998) *Cell 95*, 771−778.
8. Ferguson, A. D., Hofmann, E., Coulton, J. W., Diederichs, K., and Welte, W. (1998) *Science 282*, 2215−2220.
9. Ferguson, A. D., Chakraborty, R., Smith, B. S., Esser, L., van der Helm, D., and Deisenhofer, J. (2002) *Science 295*, 1715−1719.
10. Gudmundsdottir, A., Bell, P. E., Lundrigan, M. D., Bradbeer, C., and Kadner, R. J. (1989) *J. Bacteriol. 171*, 6526−6533.
11. Cadieux, N., and Kadner, R. J. (1999) *Proc. Natl. Acad. Sci. U.S.A. 96*, 10673−10678.
12. Merianos, H. J., Cadieux, N., Lin, C. H., Kadner, R., and Cafiso, D. S. (2000) *Nat. Struct. Biol. 7*, 205−209.
13. Cadieux, N., Bradbeer, C., and Kadner, R. (2000) *J. Bacteriol. 182*, 5954−5961.
14. Coggshall, K. A., Cadieux, N., Piedmont, C., Kadner, R., and Cafiso, D. S. (2001) *Biochemistry 40*, 13946−13971.
15. Usher, K. C., Ozkan, E., Gardner, K. H., and Deisenhofer, J. (2001) *Proc. Natl. Acad. Sci. U.S.A. 98*, 10676−10681.
16. Hubbell, W. L., Gross, A., Langen, R., and Lietzow, M. A. (1998) *Curr. Opin. Struct. Biol. 8*, 649−656.
17. Hubbell, W. L., Cafiso, D. S., and Altenbach, C. A. (2000) *Nat. Struct. Biol. 7*, 735−739.
18. Hubbell, W. L., and Altenbach, C. (1994) *Curr. Opin. Struct. Biol. 4*, 566−573.
19. Mchaourab, H., Lietzow, M., Hideg, K., and Hubbell, W. (1996) *Biochemistry 35*, 7692−7704.
20. Columbus, L., Kalai, T., Jeko, J., Hideg, K., and Hubbell, W. L. (2001) *Biochemistry 40*, 3228−3846.
21. Columbus, L., and Hubbell, W. L. (2002) *Trends Biochem. Sci. 27*, 288−295.
22. Mchaourab, H. S. (1998) *Biochemistry 37*, 12681−12688.
23. Klug, C., Su, W., and Feix, J. (1997) *Biochemistry 36*, 13027−13034.
24. Wimley, W. C. (2002) *Protein Sci. 11*, 301−312.
25. Bassford, P. J. J., and Kadner, R. J. (1977) *J. Bacteriol. 132*, 796−805.
26. Ollivon, M., Lesieur, S., Grabielle-Madelmont, C., and Paternostre, M. (2000) *Biochim. Biophys. Acta 1508*, 34−50.
27. Parente, R. A., and Lentz, B. R. (1984) *Biochemistry 23*, 2353−2362.
28. Jackson, M. L., and Litman, B. J. (1985) *Biochim. Biophys. Acta 812*, 369−376.
29. Marassi, F. M., Shivers, R. R., and Macdonald, P. M. (1993) *Biochemistry 32*, 9936−9943.
30. Altenbach, C., Flitsch, S. L., Khorana, G., and Hubbell, W. L. (1989) *Biochemistry 28*, 7806−7812.
31. Farahbakhsh, Z. T., Altenbach, C., and Hubbell, W. L. (1992) *Photochem. Photobiol. 56*, 1019−1033.
32. Altenbach, C., Yang, K., Farrens, D., Farahbakhsh, Z., Khorana, H., and Hubbell, W. (1996) *Biochemistry 35*, 12470−12478.
33. Altenbach, C., Greenhalgh, D. A., Khorana, H. G., and Hubbell, W. L. (1994) *Proc. Natl. Acad. Sci. U.S.A. 91*, 1667−1671.
34. Liang, Z., and Freed, J. H. (1999) *J. Phys. Chem. B 103*, 6384−6396.
35. Bracken, C., Carr, P. A., Cavanagh, J., and Palmer, A. G. (1999) *J. Mol. Biol. 285*, 2133−2146.
36. Crump, M. P., Spyracopoulos, L., Lavigne, P., Kim, K. S., Clark-Lewis, I., and Sykes, B. D. (1999) *Protein Sci. 8*, 2041−2054.
37. Duggan, B. M., Dyson, H. J., and Wright, P. E. (1999) *Eur. J. Biochem. 265*, 539−548.

BI0259397